Available online at www.sciencedirect.com
ScienceDirect
Journal of the European Ceramic Society 28 (2008) 1405–1419
www.elsevier.com/locate/jeurceramsoc

The influence of oxides on the performance of advanced gas turbines

A.G. Evans *, D.R. Clarke, C.G. Levi

Materials Department, University of California, Santa Barbara, Santa Barbara, CA 93106-5050, USA

Available online 28 January 2008

Abstract

Zirconia and alumina have been successfully incorporated into turbines used for propulsion and power generation. They exert a crucial influence on the fuel efficiency. The roles of these oxides within the overall system are described, relative to those for the other constituents, and their most important properties are outlined. The mechanisms that govern their properties are presented and approaches for adjusting them in desirable directions are discussed. Opportunities for new materials with potential for superior performance are assessed.

Keywords: Thermal barrier coatings; Alumina; Zirconia; Interfaces; Thermal properties

1. The motivation

Oxides are present in turbines used for propulsion and power generation. Their benefits are manifest in a substantial increase in the longevity of various hot section components.[1–8] The technology demonstrates how oxides can be used to protect structural members that experience environmental extremes. Documenting the principles that underlie this success facilitates dissemination to other systems. The technology involves choices of materials and spatial configurations, as well as survivability upon extreme temperature cycling without loss of functionality.

1.1. Materials and configurations

The following considerations have motivated the choice of materials and their spatial configurations. The *thermal requirements* are straightforward (Fig. 1). By directing air through channels, the structural alloy is internally cooled: with heat transfer coefficient determined by the flow rate and the channel geometry. Subject to a combustion temperature, T_{gas}, and an external heat transfer coefficient, superposing an *external insulting oxide* allows T_{gas} to be raised while retaining the alloy at an allowable maximum temperature. Remarkably, insulating oxides deposited onto geometrically complex structural components, such as airfoils, remain attached for extended periods despite cycling through an enormous temperature range (in excess of 1200 °C) within an oxidizing environment. A single material would be *incapable* of satisfying these requirements. The viable solution is an oxide/metal multilayer (Fig. 2). The outer oxide imparts thermal protection: while the metallic layer (bond coat) affords oxidation protection through the formation of a second oxide, as well as plastic accommodation of strain.[1–8]

At the technology inception, *the preferred insulating oxide* was determined to be yttria-stabilized zirconia (YSZ), chosen because of its low, temperature-invariant, thermal conductivity[9] (Fig. 3a). The most desirable phase was ascertained by conducting laboratory-based thermal cycle tests to seek the composition affording greatest durability: that is, the largest number of cycles before the coating spalls (Fig. 3b).[16] The outcome was 7 wt.% yttria-stabilized zirconia (7-YSZ). This composition is still used, despite the discovery of lower thermal conductivity options.[4,17–20] It remains the material of choice because other properties (especially toughness[21–25]) are also crucial. On rotating components, the layer thickness is important. It is a compromise between having sufficient thickness to achieve the desired temperature drop, yet thin enough to avert excessive inertial loads, due to the extra mass. The outcome is thickness in the range $100 \leq H_{tbc} \leq 250\ \mu m$. On stationary components, such as shrouds and combustors, the mass is less critical and much thicker layers can be used. The choice is typically, $500\ \mu m \leq H_{tbc} \leq 1$ mm.

The principles governing the materials for *oxidation protection* are straightforward: albeit with nuanced implementation. (i) A thermally grown oxide (TGO) forms at the bond coat surface by reaction with the combustion gas. The preferred TGO should have the lowest possible oxygen ingress at the temper-

* Corresponding author.
E-mail address: agevans@engineering.ucsb.edu (A.G. Evans).

0955-2219/$ – see front matter © 2007 Elsevier Ltd. All rights reserved.
doi:10.1016/j.jeurceramsoc.2007.12.023

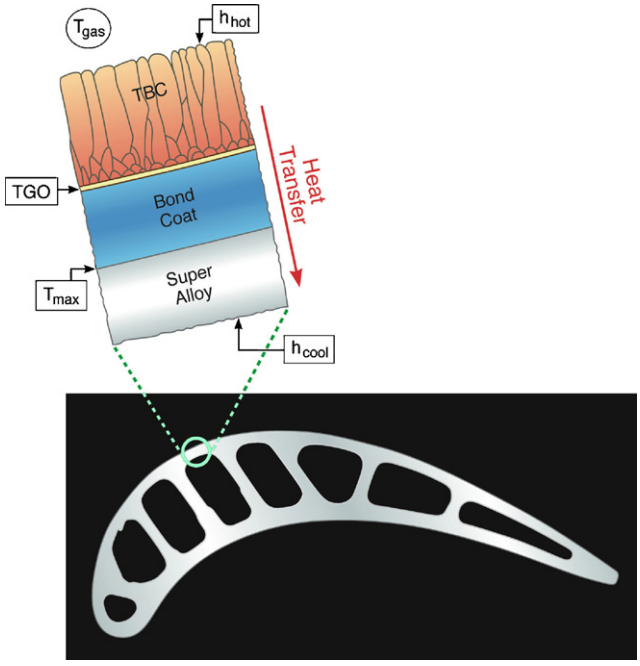

Fig. 1. A schematic of an airfoil and a magnified view of a surface zone with the TBC and bond coat layers identified. The thermal conditions are defined.

atures of interest (900–1150 °C), with correspondingly small counter-diffusion of the metallic elements. (ii) The bond coat should have sufficient thermo-chemical compatibility with the structural alloy that the basic composition, microstructure and properties are retained for the expected life of the system. *The singular solution is an alloy that forms* α-Al_2O_3 *upon oxidation*. To achieve this, near its surface, the alloy must contain sufficient Al that the primary oxidation product is, indeed, α-Al_2O_3 and, moreover, acts as a reservoir for re-formation of α-Al_2O_3 should spallation occur. The common choices are alloys based on Ni(Al) with various additions (such as Cr, Co, Pt, Y and Hf). Other requirements are more nuanced. They dictate competitive advantage, through key aspects of system performance and durability. In practice, three categories of bond coat have been implemented, differentiated by the phases present and the alloy additions. (a) One category consists of a single β-phase usually made by inter-diffusing Al and Pt with Ni adjacent to the surface of the superalloy.[26–28] (b) A second consists of a two-phase, γ/β-alloy, usually deposited onto the substrate by plasma spraying or EB-PVD.[29–31] (c) The third is a two-phase γ/γ′ alloy made by infusing Pt (and Hf) into the substrate.[32,33] Systems made using these bond coats perform differently with durability governed by different mechanisms.

1.2. Performance and durability

To survive extreme thermal cycling the *misfit strains* between the layers must be understood and managed.[34–39] These strains arise due to differences in thermal expansion coefficient, as well as phase transformations and inter-diffusion. They cause residual stresses upon temperature cycling, which activate inelastic mechanisms that, in turn, limit durability. The importance of the misfit differs for each of the layers. It is least important for the external oxide because this layer need not be dense: it serves only to insulate the underlying alloy and does not provide oxidation protection. It is designed with a microstructure having spatially configured porosity that affords low in-plane stiffness and strain tolerance.[40–44] This strategy cannot be used for either the TGO or the bond coat: because, to serve their functions, both need to be dense (minimal porosity). The TGO misfit cannot be independently controlled, but its adverse consequences can be managed by limiting its thickness. The misfits between the bond coat and substrate are more nuanced: they occur not only from thermal expansion, but also phase transformations[39] and swelling.[45] Understanding these misfits, ascertaining their importance to system durability, and finding means to control them, has been an important research focus.

Ultimately the durability is governed by spalling of the external insulating oxide, as deduced from components removed from engines (Fig. 4). Small diameter spalls can be tolerated, because backside cooling and boundary layer effects still allow the exposed surface to be protected by the (surrounding) intact oxide. Degradation only becomes a concern after an appreciable area fraction of the coating has been removed. Actual spall formation is preceded by smaller cracks that extend and coalesce along delamination planes located either within the oxide layer or at the interface between the TGO and the bond coat.

The ensuing article highlights the roles of the oxide constituents. It is organized as follows. The constituent materials and their salient thermo-mechanical properties are outlined. The spectrum of mechanisms governing the performance and durability of hot section components are described, thereby illuminating the oxide functionalities. With reference to these mechanisms, the dominant characteristics of the oxides are discussed, with associated mechanistic understanding. In turn, these mechanisms reveal opportunities for new research on oxides that might further enhance the fuel efficiency.

2. The constituents and their thermo-mechanical properties

The requirements imposed on each layer (Fig. 2) dictate the constituent property attributes. In current implementations, the structure and composition of the substrate and the insulating oxide are largely fixed. Options exist for the bond coat, which affect the formation of the ensuing TGO.

2.1. Insulating oxide

The thermal expansion coefficient of this layer, α_{tbc}, is appreciably lower than that for the substrate, α_{sub}: the difference is about, $\alpha_{tbc} - \alpha_{sub} \equiv \Delta\alpha_{tbc} \approx -3$ ppm/K. To prevent spontaneous delamination due to this misfit, the in-plane modulus of the layer, E_{tbc}, must be controlled, as illustrated by the following simple argument. At the highest temperature, creep in the YSZ causes it to become stress-free. Subsequent cooling induces residual stress through the thermal expansion misfit. If the YSZ were fully dense ($E_{tbc} = 200$ GPa, $\nu_{tbc} \approx 0.2$), for a typical value of the average temperature

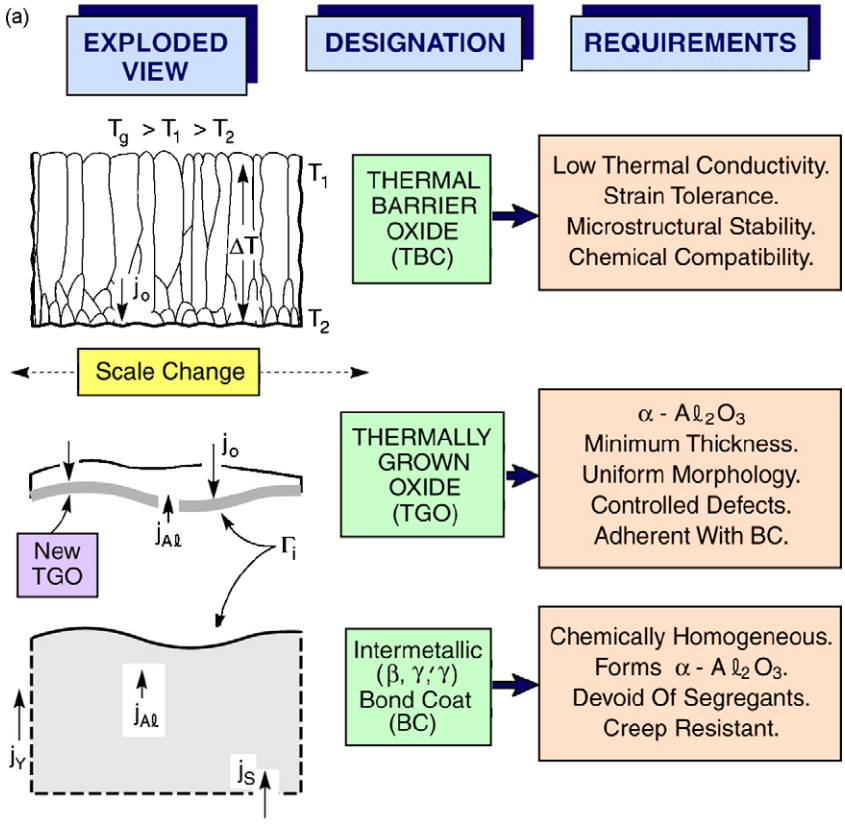

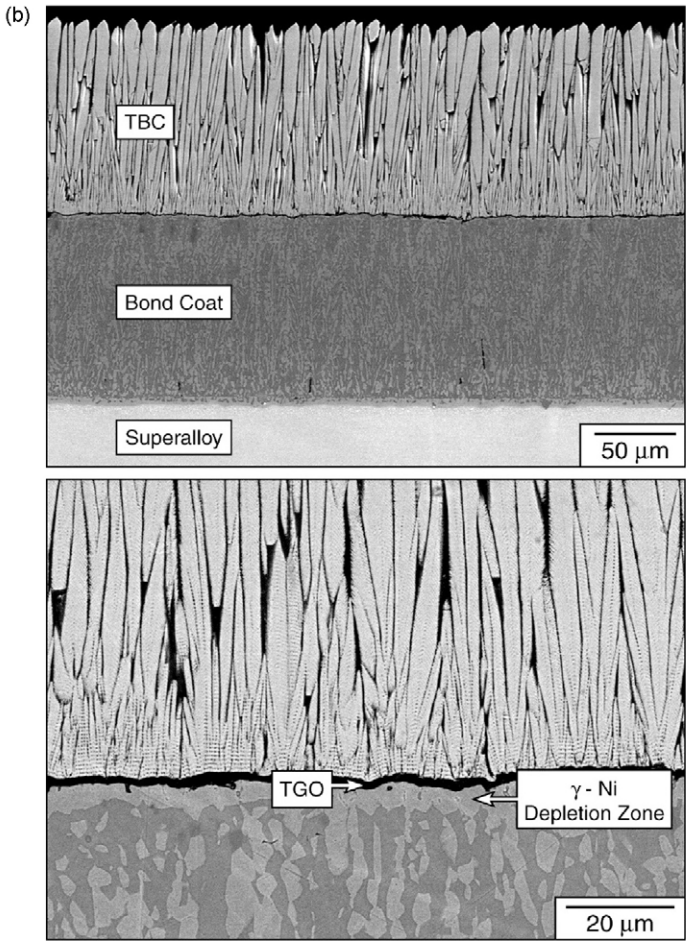

Fig. 2. An exploded view of the tri-layer thermal barrier system indicating the functionalities of each of the layers. Cross sections of actual systems are included.

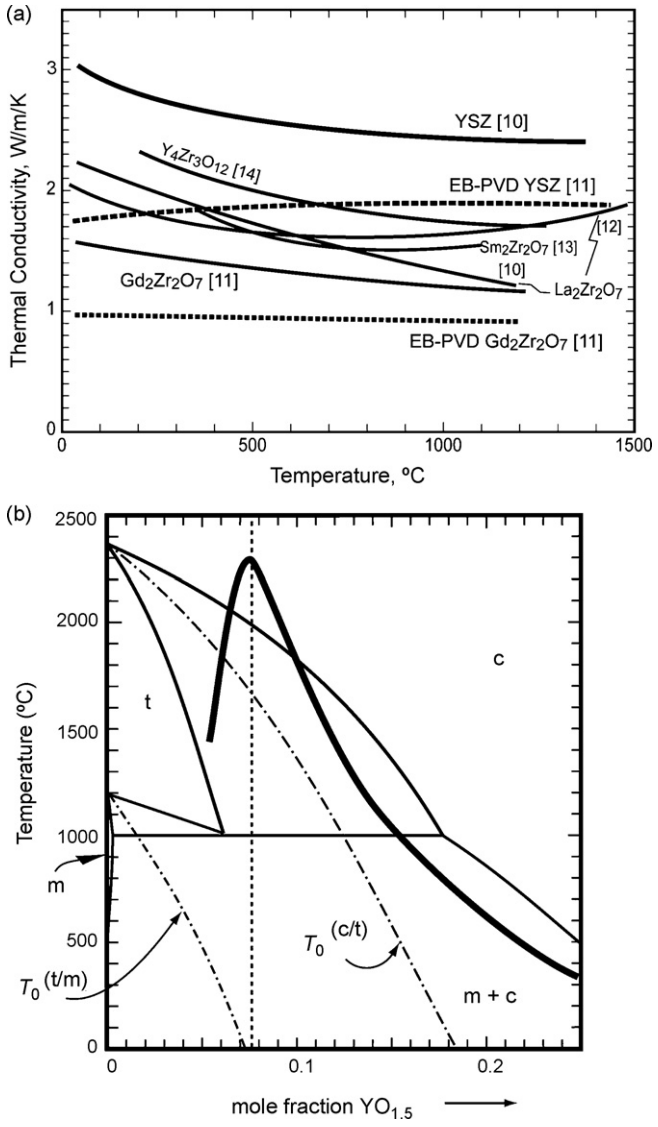

Fig. 3. (a) The thermal conductivity of several insulating, ternary oxides as a function of temperature.[10–14](b) A binary phase diagram for the ZrO_2–$YO_{1.5}$ system showing the phases expected.[15] A line representative of the cyclic durability is superposed.[16]

drop ($\Delta T \approx 1100\,^{\circ}C$), the residual stress at ambient would be, $\sigma_R \approx E_{tbc}\Delta\alpha_{tbc}\Delta T/(1-\nu_{tbc}) \approx -0.8$ GPa. For thickness, $H_{tbc} \geq 100\,\mu m$, the stored energy/area, $U_{tbc} \equiv \sigma_R^2 H_{tbc}/2E_{tbc} \geq 160\,J/m^2$, would substantially exceed the mode I toughness ($\Gamma_{tbc} \approx 45\,J/m^2$ for 7-YSZ[23]), rendering the system prone to spontaneous delamination.[22] To obviate this problem, deposition methods have been developed that create a non-dense microstructure with appreciably lower in-plane modulus, $E_{tbc} \leq 50$ GPa.[40,41] In this modulus range, the stored energy becomes of order the toughness (typically, $U_{tbc} \approx 45\,J/m^2$ for $H_{tbc} = 150\,\mu m$), enabling implementation. The columnar structure developed by EB-PVD is especially effective.[42]

2.2. Bond coat

The relationships between the properties of the bond coat and system durability are much more nuanced, because of the highly non-linear interplay with the substrate and the TGO.[36,37] The "ideal" bond coat would have the following attributes: (i) resistant to inter-diffusion with the substrate, (ii) minimal strain misfit with the substrate (based on thermal expansion, phase transformations and minimal inter-diffusion-induced swelling) and (iii) high creep strength with adequate ductility. All of these preferences cannot be realized simultaneously. The challenge has been to identify those attributes having the greatest importance.

2.3. Thermally grown oxide

The characteristics of the TGO are controlled largely by the bond coat microstructure and microchemistry, but modulated by impurities, water vapor and dopants. Upon initial oxidation, transient phases of alumina generally form. Later, these convert into α-Al_2O_3.[46–53] The bond coats used in practice develop this phase at a relatively early stage within the cyclic life, minimizing adverse influences of the phase transformation on durability. As the α-Al_2O_3 layer grows, it develops a small (but significant) compressive stress.[54,55] Upon cooling, the compression increases dramatically, due to thermal expansion misfit with the substrate: $\alpha_{tgo} - \alpha_{sub} \equiv \Delta\alpha_{tgo} \approx -7$ ppm/K, such that $\sigma_{tgo} \approx -4$ GPa at ambient.[56–58] Consequently, even though the TGO may be relatively thin at the end of the cyclic life ($h_{tgo} \approx 6\,\mu m$), the energy stored/area is quite large, $U_{tgo} = \sigma_{tgo}^2 h_{tgo}/2E_{tgo} \approx 80\,J/m^2$ and contributes substantially to the potential for delamination at the TGO/bond coat interface (Fig. 5).

2.4. Interfaces

While interfaces between metals and oxides involve fundamentally strong (covalent and ionic) bonds,[59–61] their adhesion can be compromised by minor impurities (S is especially detrimental).[61] To inhibit such degradation, there has been a long history in the industry of systematically lowering the S level in superalloys, as well as using selected alloy additions (Y, Pt, Hf, etc.) to tie-up remnant S.

3. Mechanisms limiting the durability of hot section components

An early challenge in the implementation of thermal barrier systems was the difficulty in realizing laboratory tests that reproduced the conditions that arise in an operating turbine. Furnace cycle and burner rig tests were widely used, but the spalling mechanisms were not always representative of those found in airfoils, shrouds or combustors removed from actual engine service. As the body of information acquired on components accumulated, this concern became less problematic. A remaining issue is the merit of purported failure mechanisms presented in the literature, obtained on specimens tested in a laboratory setting. To eliminate the concern, each of the mechanisms presented below has been carefully scrutinized and correlated with engine experience. Namely, the mechanisms are those that the authors deem reproducible and verifiable, on the basis of engine

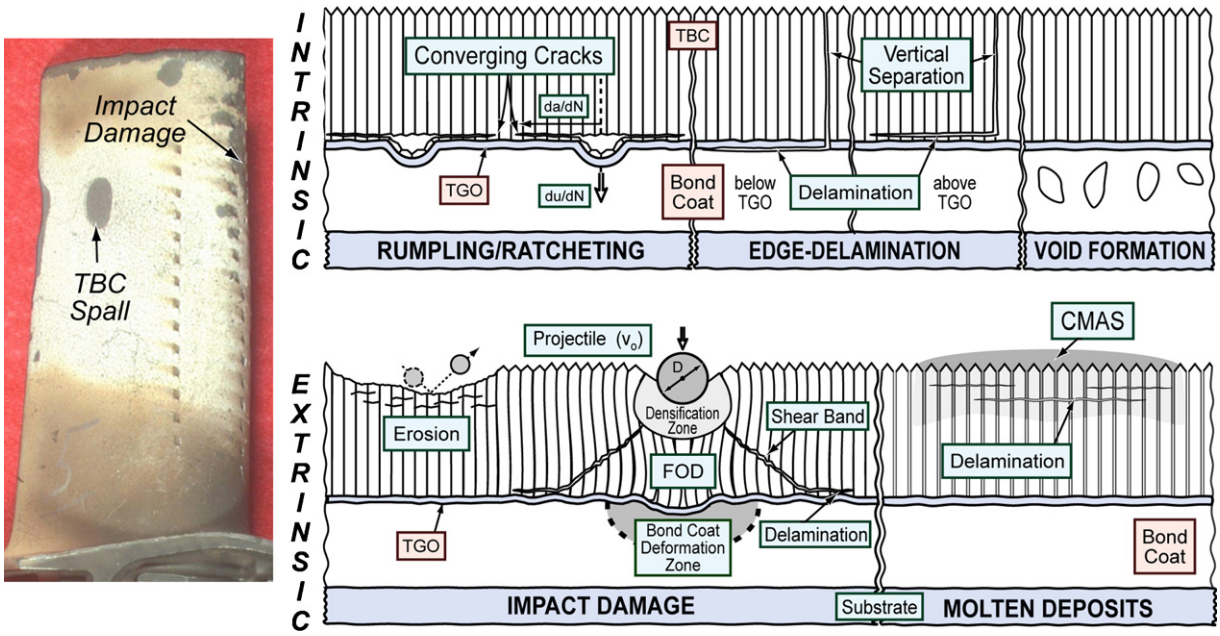

Fig. 4. A summary of the various mechanisms that can cause spalling of the TBC on turbine airfoils. The intrinsic mechanisms are governed by strain misfits between the constituent layers upon thermal cycling. The extrinsic mechanisms are determined by external factors. Also shown at the left is an airfoil removed from engine service that contains various spalled regions.

experience. They reside within two basic categories: intrinsic and extrinsic (Fig. 4). Those in the intrinsic category are not especially sensitive to the presence of a thermal gradient in the component and *vice versa*. *The intrinsic category* is characterized by a group of mechanisms that arise because of the strain misfits associated with the constituent materials. These mechanisms can often be reproduced in well-executed furnace cycle and burner rig tests. The failures are ultimately manifest as spalls, usually present in hot sections. In systems with *EB-PVD coatings*, three different intrinsic mechanisms have been identified, differentiated in terms of the surface exposed by the spall. (i) One mechanism exposes zirconia and some alumina on both delamination surfaces. Cross sectioning indicates that it is accompanied by rumpling (or ratcheting) of the TGO, manifest as undulations that, locally, penetrate into the bond coat (Fig. 6).[62–64] This mechanism arises primarily in systems with β-phase bond coats. (ii) A second exposes the bond coat, with periodic islands of TGO and some entrained zirconia. The bond coat exhibits imprints of the grains in the TGO, suggesting brittle failure by loss of adhesion at the metal/oxide interface. Cross sections affirm that the failure occurs primarily by delamination along the interface, with local extension through thickness heterogeneities in the TGO (Fig. 7).[31] (iii) A third exposes the bond coat, but now with superposed features indicative of voids formed at longer times.[65] All intrinsic mechanisms have a characteristic TGO thickness, h_{crit}, at the incidence of spalling. However, h_{crit} depends on the bond coat composition and microstructure, as well as the thermal cycling history. In itself, it is not an useful metric for characterizing failure across a range of bond coats and cycling scenarios. *The extrinsic category* cannot be reproduced in furnace cycling or conventional burner rig tests. The mechanisms include damage induced by particle impact (erosion and foreign object damage),[66–69] delaminations enabled by the penetration of deposits of calcium–magnesium–aluminosilicate (CMAS) formed from the ingress into the engine of sands and dust in the atmosphere[70–72] as well as those introduced by thermal gradients.[21] All are dominated by the microstructure and properties of the insulating oxide. The manifestations in turbine hardware are as follows. Foreign object damage (FOD) is apparent as spalls at the leading edges of airfoils. Less severe particle impacts cause the gradual thinning of the TBC, by erosion: also in the vicinity of the leading edges. CMAS damage

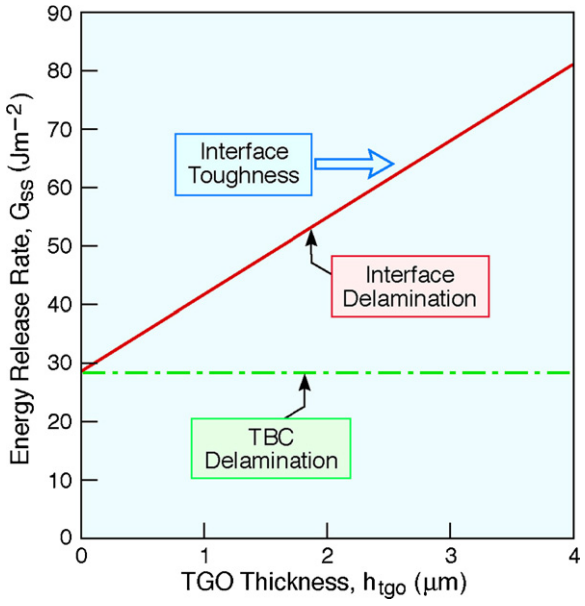

Fig. 5. The energy release rates for delamination along either the TGO/bond coat interface, as a function of TGO thickness, or internally, within the TBC. Also shown is an estimate of the mode II toughness of the interface.

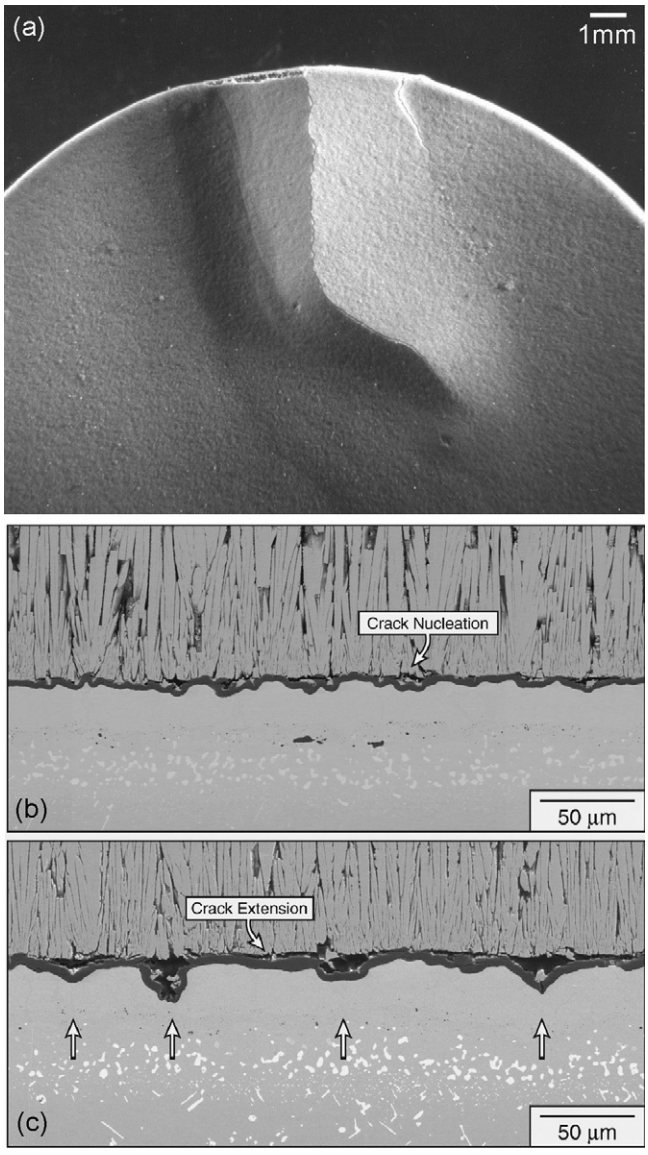

Fig. 6. (a) A large-scale buckle in a TBC coating with a ridge crack along the top. This buckle initiated at the upper-free edge. (b and c) Cross sections away from the buckle revealing the development of multiple (small) cracks in the TBC above the TGO.

is found in the hottest sections of airfoils, especially along the pressure surface, and in shrouds. Once molten, the CMAS is evident through a yellow coloration associated with transition elements (such as Fe and Mn), in the deposits. The mechanism operates in the presence of a thermal gradient that plays a dual role.[21] (a) It enables the CMAS (once molten) to penetrate to a specified depth into the oxide. (b) It causes the surface to experience residual tensile stress upon cooling.[72] In turn, these stresses provide the energy release rate, G, that enables internal delamination (substantially elevated by the increase in stiffness caused by CMAS penetration). Because it has not yet been possible to adequately duplicate these mechanisms in laboratory scale tests, the mechanistic understanding has been based on observations and measurements made on components removed from engines. The implementation of new testing facilities will rectify this shortcoming.

The pre-eminent influences of the oxide constituents emerge in the context of the foregoing mechanisms. The *alumina influences all of the intrinsic mechanisms*. When the spalling is dictated by rumpling of the TGO, three of the most important influences are attributed to the alumina: (a) its thickening rate, (b) the magnitude of the stress induced as it thickens and (c) the thermal expansion misfit with the substrate. Small values of all three are most desirable. The microstructure and properties of the *insulating layer have greatest influence upon the extrinsic mechanisms*. The salient properties include: (a) the toughness, (b) the yield strength at high temperature, (c) the in-plane modulus and (d) its densification rate. The incidence and extent of all of the cracking and delamination mechanisms scale directly with the toughness. Indeed, a central attribute of 7-YSZ is its relatively high toughness. The yield strength plays a role through the ability of plasticity to dissipate the kinetic energy from particles circulating in the turbine that impinge onto the rapidly rotating airfoils. The modulus affects the level of residual stress induced as the system thermally cycles because of the thermal expansion misfit with the substrate. In turn, the modulus is affected by the microstructure, established by the method of deposition, and modified by sintering or CMAS penetration.

4. The role of the alumina

4.1. Thickening and elongation

Over the thickness range that dominates intrinsic durability, the salient phenomena are dictated by the α-Al_2O_3 phase with columnar grain structure (Fig. 8). At the temperatures of interest (1000–1125 °C), the growth involves counter-diffusion of oxygen and aluminum along the α-Al_2O_3 grain boundaries (Figs. 8 and 9).[73] The diffusion flux, and hence, the parabolic rate constant, is dictated by the grain size of the α-Al_2O_3 as well as by impurities and by dopants that diffuse to the TGO and become entrained. While there is a wealth of empirical data on this topic, the fundamentals remain elusive. Two issues are critical:

(i) Phase transformation from amorphous alumina (formed during initial stages of heating) through various transient polymorphs to the stable α-Al_2O_3. The rate of transformation determines the nucleation rate of the stable phase, as well as its lateral growth rate. In turn, this determines the grain size of the α-Al_2O_3, thereby controlling the subsequent thickening rate (as oxidation proceeds by grain boundary diffusion). The α-Al_2O_3 forms by means of a nucleation and growth process. Understanding the role of certain dopants on this process is important because (a) Cr is always incorporated for corrosion resistance and (b) rare earths such as Hf and Y are used to control interface adhesion, as well as the rumpling propensity (discussed below). It is known that doping with Hf and Y retards the growth rate of the α-Al_2O_3 once nucleated. This benefit happens because these large cations are soluble in gamma and theta but not in alpha, causing them to be rejected from the growing α. Consequently, the interface cannot advance into the

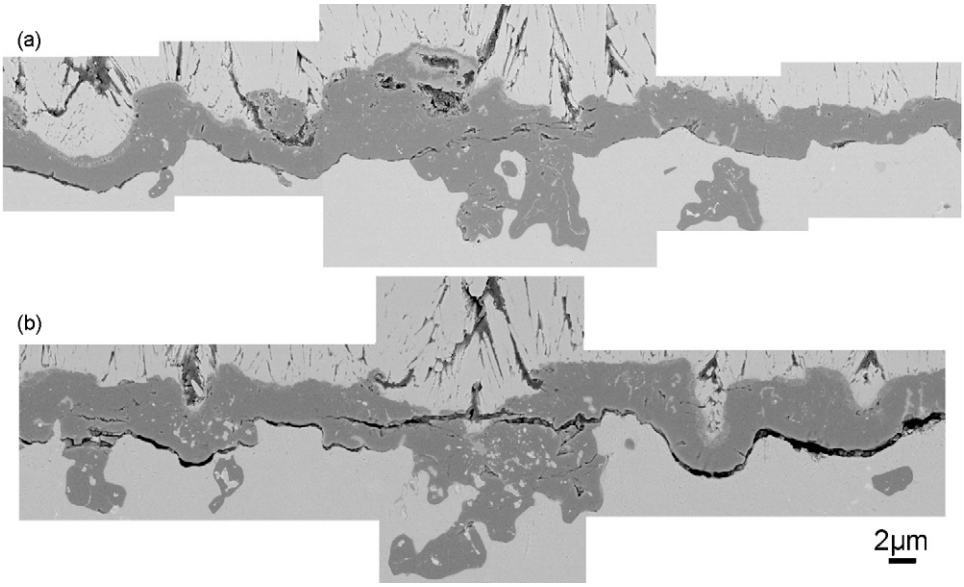

Fig. 7. Cross sections through a burner rig test specimen comprising an MCrAlY bond coat after thermal cycling to full life. (a) A section remote from the spalled region showing the intact interface. (b) A region adjacent to the spalled zone showing that the delamination follows the interface except where it extends across a thickness heterogeneity.

metastable phase until the excess solute precipitates, since the local driving force is insufficient. Conversely, Cr and Fe (cations soluble in α) accelerate the growth rate: a feature elucidated by polishing the surface of bond coat alloys with Cr and Fe oxides and noting preferential growth of alumina on heterogeneous nuclei created at the polishing features (scratches, grit-blast grooves, etc.) (Fig. 10). Given these counteracting influences of the dopants, a compromise in the relative dopant levels is required. However, because a quantitative model is lacking, reliance has been placed on empiricism, with adverse consequences for progress toward optimal doping strategies.

(ii) The relative inward and outward diffusive fluxes along the grain boundaries in the ensuing α-Al_2O_3 influences both thickening and elongation. The grain boundaries governing these effects are clean and devoid of amorphous interphases (although sub-monolayers of Hf or Zr can be entrained). The conventional picture is that, once α-Al_2O_3 is formed, oxide thickening is dominated by inward diffusion of O. In practice, there is a counter-flux of cations,[73,74] demonstrated by using the following protocol. The alloy is oxidized to form a continuous TGO, which is then polished at an angle, and re-oxidized. Some of the new oxide forms as ridges along locations where the oxide grain boundaries intersect the surface (Fig. 9). There are corresponding ridges where the grain boundaries intersect the interface. Measurement of the volume of these ridges allows assessment of the relative anion and cation fluxes (note that, in Fig. 9 the inward and outward fluxes must be of comparable magnitude). Such measurements reveal that the counter-fluxes depend sensitively on dopants such as Hf and Y entrained in the grain boundaries of the growing oxide. The unresolved question is how to think about the atomic mechanisms of counter-diffusion, and how this process determines elongation strain. These fundamentals have not been addressed in the literature.

4.2. The stresses in the TGO

If all of the new α-Al_2O_3 formed at the interface with the bond coat, the ensuing volume increase would be accommodated by upward (rigid body) motion of the prior TGO, obviating a growth stress. Instead, the outward counter-flux of Al causes some new α-Al_2O_3 to form at dislocations/ledges along the transverse grain boundaries, as well as that formed on the surface of the TGO (Fig. 9). That formed at the boundaries must be accommodated by lateral deformation of the neighboring grains, causing a compressive growth stress (Fig. 11). Since α-Al_2O_3 is susceptible to plastic deformation at the growth temperature, the stress attains a "steady-state", wherein the strain-rate induced by the growth is balanced by the creep-rate. The magnitude of this stress has been measured *in situ* for the TGO formed on several different bond coats. It is measured to be of order, $\sigma_{growth} \approx -300$ MPa[54] (Fig. 12). While this stress level appears reasonable based on deformation mechanism maps for α-Al_2O_3 and stress relaxation rates in a typical TGO, it remains to develop a quantitative model. Moreover, the influences of role of dopants on growth strains and relaxations are poorly understood. Upon cooling, because of its relatively low thermal expansion coefficient (relative to the substrate) a large in-plane compression develops (Fig. 12). At ambient, whenever the TGO remains planar (no rumpling), the compressive stress is in the range, $-3.5 < \sigma_{tgo} < -6$ GPa, depending on the thermal expansion coefficient for the substrate.[58] When rumpling occurs, the stress diminishes, because of bending and elongation of the TGO.[37,57]

Rumpling is highly non-linear phenomenon, involving interactions between the TGO, bond coat and substrate and reliant on many thermo-mechanical properties of the layers. The interactions have been unearthed through the development of a code and its validation by incisive experiments.[36] While the rumpling rate is strongly influenced by the strain misfits between the sub-

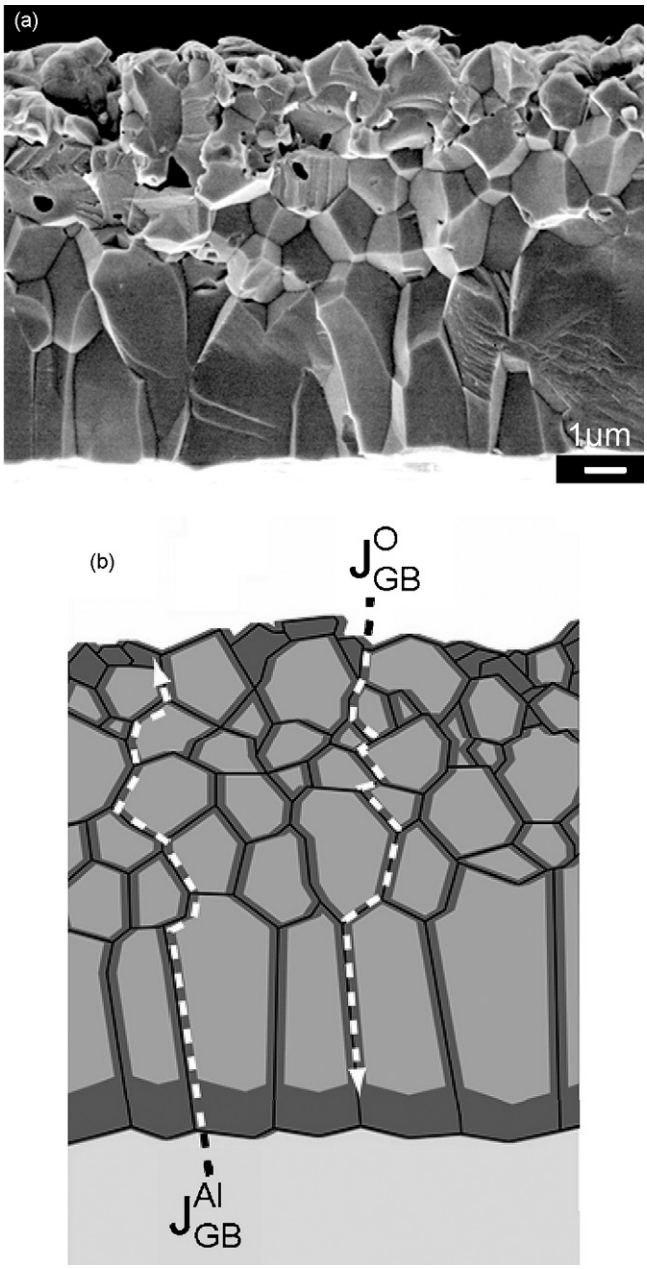

Fig. 8. (a) Fractured cross section of a TGO illustrating the inner, columnar portion of the oxide formed by inward diffusion of O and the outer, equiaxed portion formed by outward diffusion of Al. (b) Schematic diagram showing the flux paths.

strate and bond coat, as well as its creep strength, the TGO is also important. From a TGO perspective, the growth stress and the thickening rate are most influential.

4.3. Interface adhesion

When rumpling is suppressed, durability is limited by delamination along the interface between the TGO and the bond coat. The energy release rate enabling this mechanism (Fig. 5) is communicated to the interface as a mode II (shear) delamination. In principle, equating the energy release rate to the mode II toughness of the interface predicts a lower bound on the TGO thickness that causes delamination (Fig. 5). In practice, this approach to predicting the critical thickness has not been realized, because the mode II toughness is a notoriously difficult property to measure. Instead, estimates based on the mode I and mixed-mode delamination toughness have been invoked. However, these results demonstrate order of magnitude variations that depend on the presence of segregants and the method used to form the interface. Instead of placing reliance solely on measurements, a simulation scheme that distinguishes the factors dominating the adhesion (Fig. 13) is being pursued. It has two basic ingredients. (i) The traction/separation characteristics during bond rupture at the interface are ascertained using a first principles approach based on density functional theory. (ii) These results are input to an embedded process zone (EPZ) simulation of interface crack extension that captures the multiplicative influence on the toughness of the plastic dissipation occurring in the bond coat. In general, the traction/separation curves are found to depend on the termination plane (stoichiometry) of the α-Al_2O_3, as well as the presence of dopants and impurities. For γ-Ni(Al) alloys, the termination has been ascertained to be a mix of stoichiometric and Al-rich. The former is the least adherent (Fig. 14). Moreover, when present, S segregates to this interface and further decreases the adhesion (by up to 70%), because the interfacial covalent-ionic Ni–O bonds are replaced with weaker ionic-covalent S–Al bonds. Doping with Hf obviates the detriment, especially when it segregates on interstitial sites (Hf_I) (Fig. 14), because Hf–Ni and Hf–O bonds effectively knit the surfaces together. When integrated (Fig. 13), these results establish a rationale for designing tough interfaces. Recall that Hf has the additional benefit that it affects the creep strength of the TGO when it segregates to the grain boundaries.

5. The insulating oxide

Beyond the basic requirement that the thermal conductivity be low and (preferably) temperature invariant, the following properties are critical to system performance. *Toughness* affects all of the extrinsic mechanisms. Remarkably, the range realizable among all (non-fibrous) oxides is fully encompassed by YSZ across the composition range between cubic and tetragonal (Fig. 15).[22] The cubic materials (c-ZrO_2 → 20-YSZ) are exceptionally brittle (toughness, $\Gamma \approx 6\,J/m^2$), while partially stabilized tetragonal materials (t-ZrO_2 → 3-YSZ), which experience a martensitic transformation to the monoclinic phase (m-ZrO_2), are among the toughest ($\Gamma > 300\,J/m^2$). The transformation mechanism is inapplicable for two related reasons. (a) It is thermodynamically forbidden at elevated temperatures, specifically those above T_0(t/m) (Fig. 16a), wherein there is no driving force for the partitionless t → m transformation. (b) Repeated cycling across the T_0(t/m) results in disruptive volume changes every time the t-ZrO_2 transforms to m-ZrO_2 on cooling and regenerates upon heating, with concomitant microcracking. Compositions within the non-transformable tetragonal (t′) phase field, bound by the compositions for which T_0(t/m) is below ambient and T_0(c/t) is below the maximum operating temperature, provide the best performance. Because tetragonality typically decreases with increasing dopant content[75] the pre-

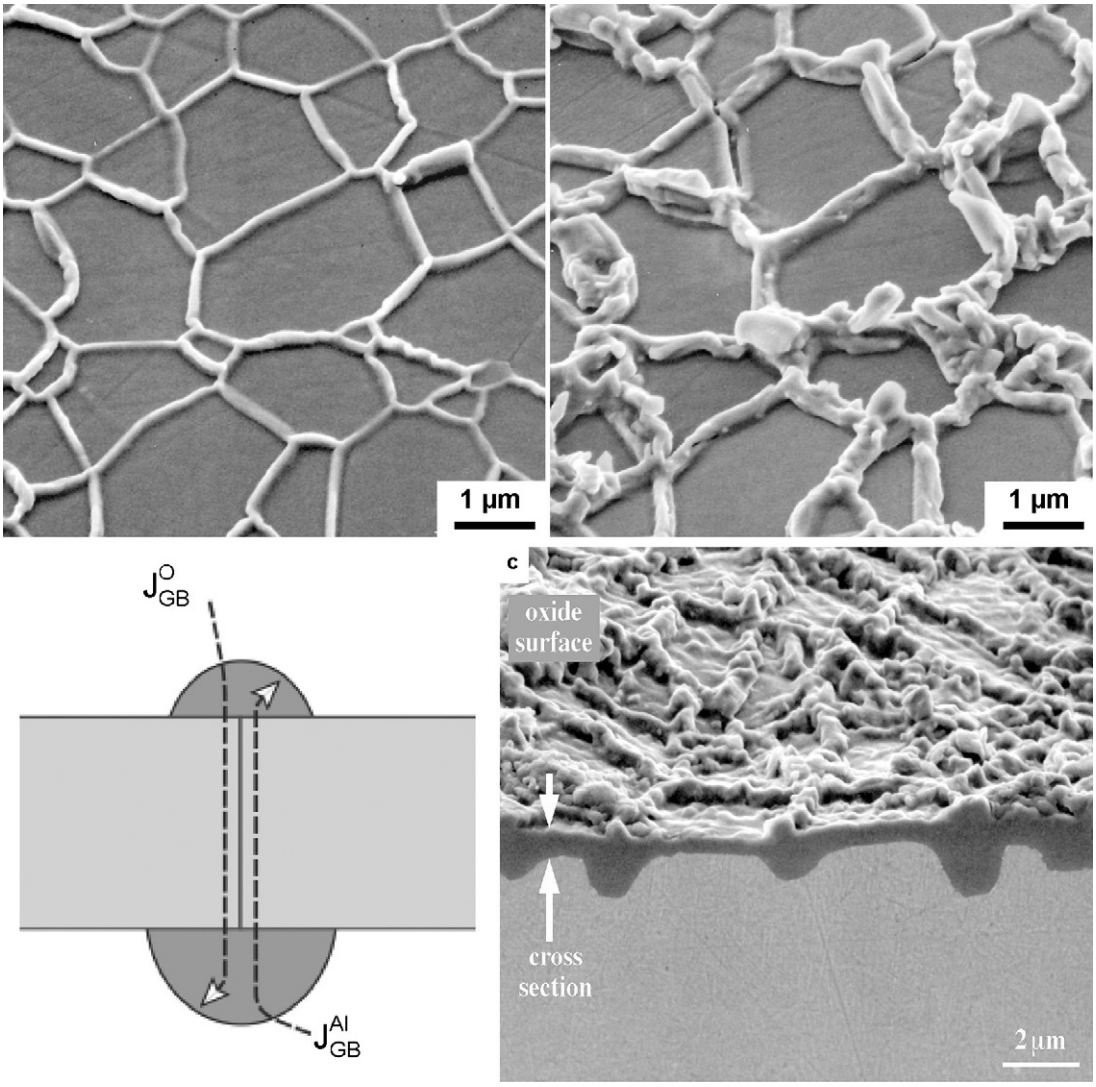

Fig. 9. Illustration of the same area of an alumina TGO on re-oxidation after smoothly polishing the TGO formed in the first oxidation step. New oxide forms along the grain boundaries of the initially formed TGO and the amount increases with further oxidation. Schematic of the counter-diffusion of O and Al along the TGO grain boundaries leading to a thickening of the oxide above and below the oxide on either side of the boundary. In between grain boundaries, the oxide is significantly thinner as indicated by the arrows.

ferred compositions within this range are those at the lower end, pre-eminently exemplified by 7-YSZ. Typically, the mode I toughness is in the range, $40 < \Gamma < 50\ J/m^2$ [23–25,76]: sufficient to prevent spalling after manufacturing and to suppress large-scale delamination when exposed to thermal gradients. Such compositions are ferro-elastic.[77–79] Upon crack extension, dissipation occurs through the formation (or switching) of nano-scale domains, resulting in toughening that scales with the tetragonality, c/a, and the coercive stress.[23,24,77–79] The concept that the tetragonality governs the toughness of tetragonal oxides has led to the development of new compositions with appreciably higher toughness than 7-YSZ.[24,25,80] The most prominent example resides within the ZrO_2–$YO_{1.5}$–TiO_2 ternary phase field (Fig. 16), having toughness, $\Gamma \approx 90\ J/m^2$ [24] (Fig. 17). *Modulus*. Given that the in-plane modulus of the layer is so important, it is remarkable that measurements are still sparse. The only comprehensive results are those published by Johnson et al.[40] Values in the range $20 < E < 40$ GPa (compared with 200 GPa for dense 7-YSZ) are representative: consistent with a microstructure comprising columns bonded at periodic attachment sites. *Yielding*. The ability of the layer to yield when impacted by foreign objects in the engine is a significant attribute. The plastic response upon impact at high temperature is reflected in the relatively low yield strength of 7-YSZ above 900 °C (Fig. 18a). The associated plastic dissipation serves to absorb much of the kinetic energy from the impact and thereby, diminish the amplitude of the elastic waves that propagate through the layer.[21] Also of interest is the role of yielding in the development of kink bands in systems having columnar microstructure (Fig. 18b). The plastic bending of the columns is apparent, as well as the incidence of cracks wherever the bending induces large tensile strains.[68,76]

As engine temperatures continue to increase, two factors will inevitably limit the capability of 7-YSZ and tetragonal compositions derived from it. One limitation arises from the metastable nature of non-transformable t' phases, since the amount of solute required for non-transformability typically

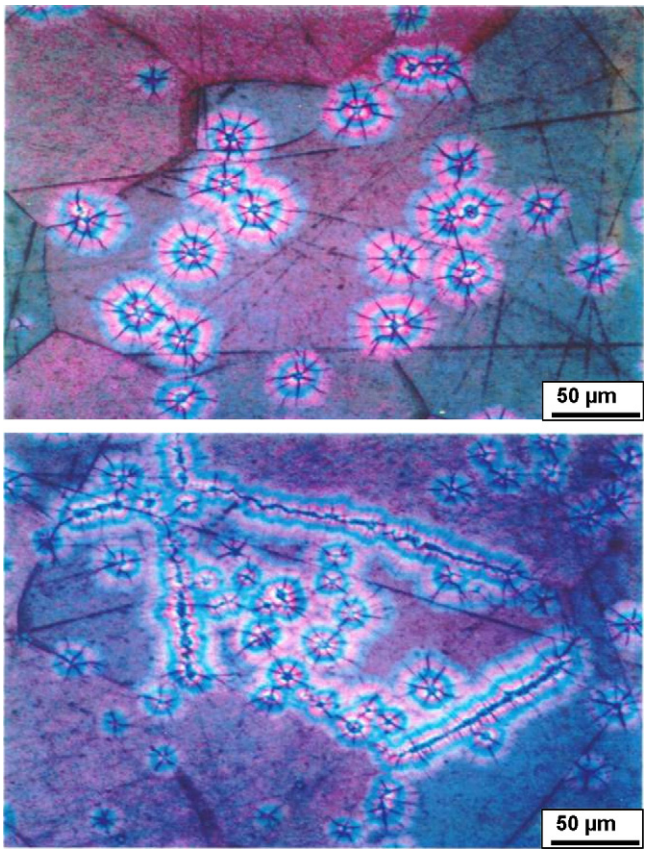

Fig. 10. Illustration of preferred nucleation of alpha-alumina islands on heterogeneous sites, such as scratches, on the alloy surface. Optical micrographs.

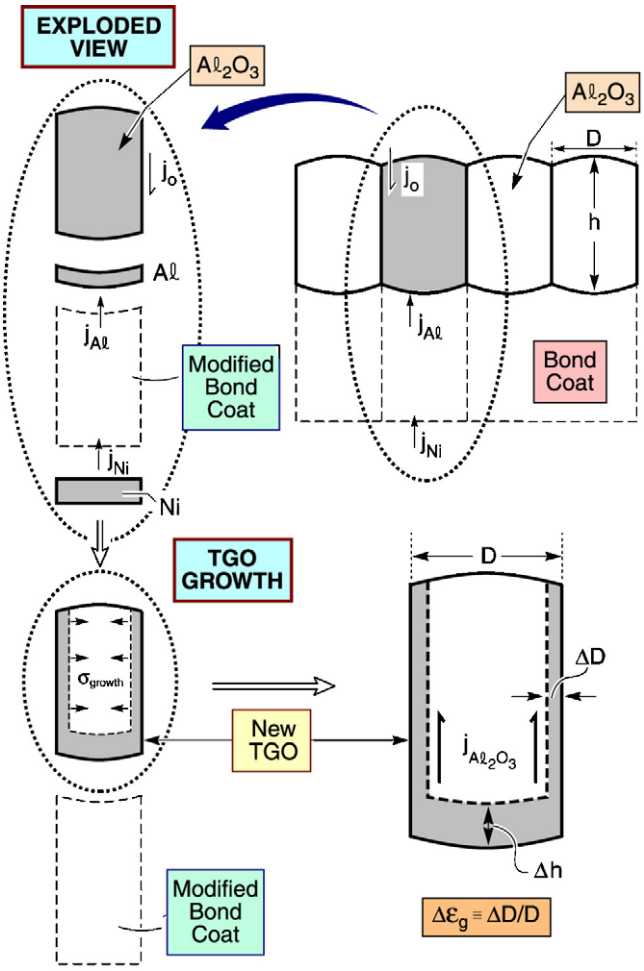

Fig. 11. A schematic indicating the elastic compression of the TGO grains needed to accommodate the formation of new alumina at the internal grain boundaries.

exceeds the solubility limit for most viable stabilizers.[4] The implication is that all these compositions have a durability ultimately limited by the partitioning of the supersaturated t' into the equilibrium phases, and the potential for undesirable transformation of the depleted tetragonal phase into monoclinic on cooling.[81–87] Small windows of opportunity exist in ternary systems. The composition exhibiting highest toughness resides in the ZrO_2–$YO_{1.5}$–TiO_2 system having a depleted tetragonal phase that is non-transformable upon cooling.[24] An interesting opportunity is presented by the ZrO_2–$YO_{1.5}$–$TaO_{2.5}$ system wherein the tetragonal field penetrates deeply into the ternary and exhibits a regime in which compositions are both immune to phase separation (up to at least 1500 °C) and also exhibit toughness comparable to (or slightly higher than) 7-YSZ.[25] This system has yet to be synthesized in coating form and evaluated for durability.

A second major limitation of 7-YSZ (and its derivative t' compositions) is the degradation by CMAS penetration.[71,72,88] Rare earth zirconates, notably $Gd_2Zr_2O_7$, offer a solution as they react with the CMAS melt and induce its crystallization at temperatures well above the melting point of the original deposit.[89] Because the reaction and crystallization kinetics are competitive with that for infiltration, the process effectively seals the surface against further penetration. However, RE zirconates are typically cubic (pyrochlore or δ-phase) and exhibit the same low toughness as cubic zirconia compositions. Moreover, they are

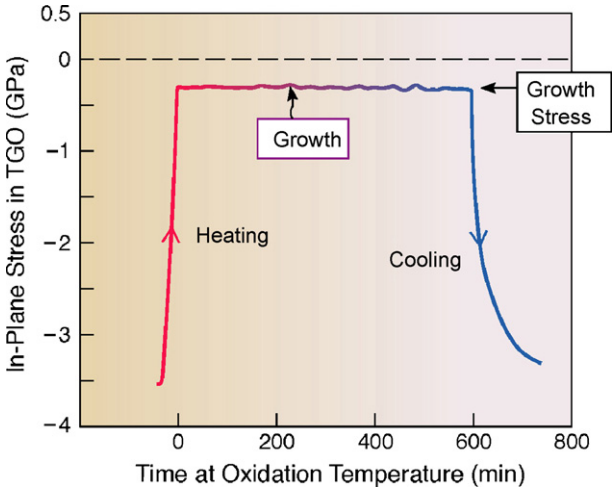

Fig. 12. An illustration of the stress in the TGO measured *in situ* in the synchrotron during a single thermal cycle from ambient to 1125 °C and back to ambient.

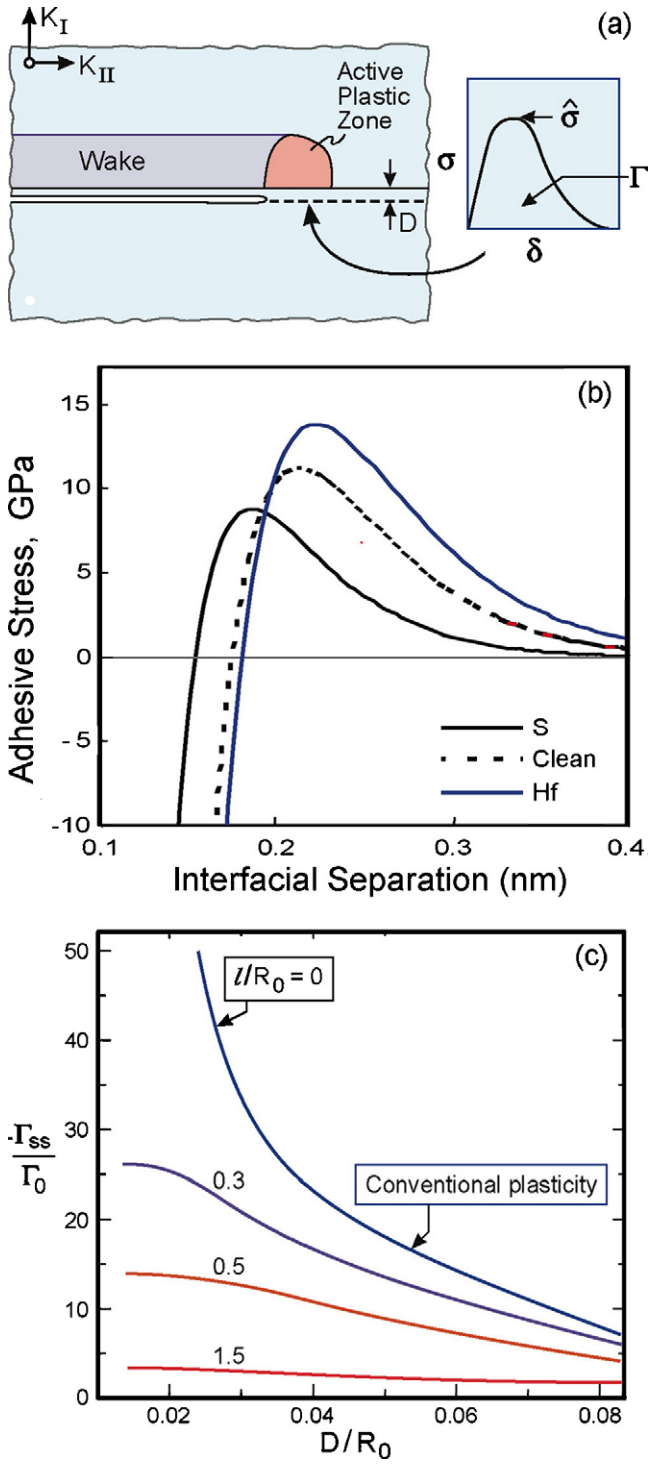

Fig. 13. (a) A schematic showing how traction/separation results (right) obtained from first principles calculations become an embedded process for a crack extension simulation that captures the multiplicative influence of plastic dissipation on the interface toughness. (b) The ratio of the toughness to the work of separation as a function of the ratio of the dislocation-free zone width, D, to the plastic zone size on the metal side of the interface, $R_0 \sim E\Gamma_0/\sigma_Y^2$, with σ_Y the yield strength and l the plasticity length scale.

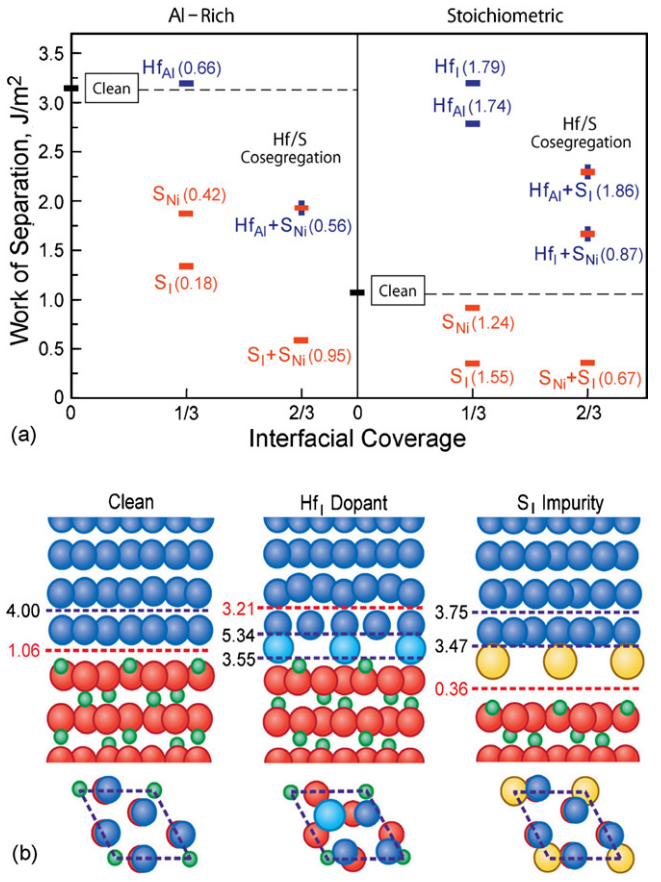

Fig. 14. (a) Trends in the work of separation calculated using density functional theory for both stoichiometric and Al-rich interfaces. (b) The atomic arrangements at a stoichiometric interface, with and without dopants and segregants. The numbers refer to the work of separation on the indicated plane (in J/m^2).

thermo-chemically incompatible with the TGO[4,90] and require a diffusion barrier to preclude deleterious interactions.[90] A suitable diffusion barrier is 7-YSZ, which also provides a tougher underlayer to hinder the propagation of cracks originating near and above the TGO. Unfortunately, solutions for toughening the zirconates are not immediately evident, and the challenge remains to be addressed by future research.

6. Research opportunities

From the foregoing synopsis the opportunities emerge for research on alumina and zirconia (and related oxides) that might further enhance in the performance of hot section components in turbines.

(i) Despite decades of research the thickening rate of the α-Al_2O_3 (once formed) remains to be understood. There are dramatic effects of impurities (detrimental) and dopants (beneficial). The grain size is also important because the diffusional fluxes occur primarily along the grain boundaries. The counter-fluxes of oxygen and Al have yet to be accounted for in the context of a viable atomistic model. This is of key importance since the latter are directly responsible

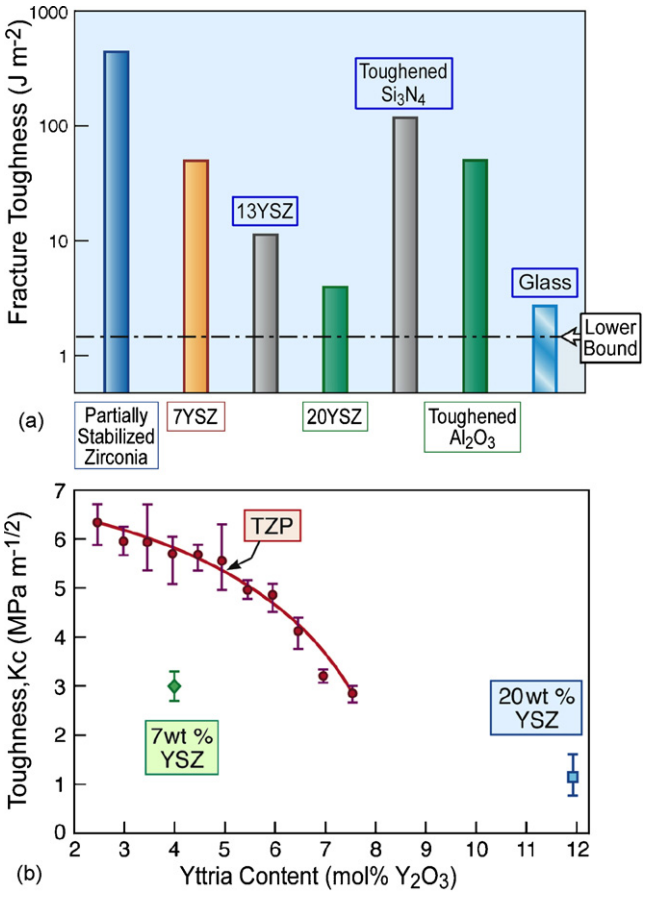

Fig. 15. The toughness of monolithic ceramics showing the wide range achievable in the YSZ system.

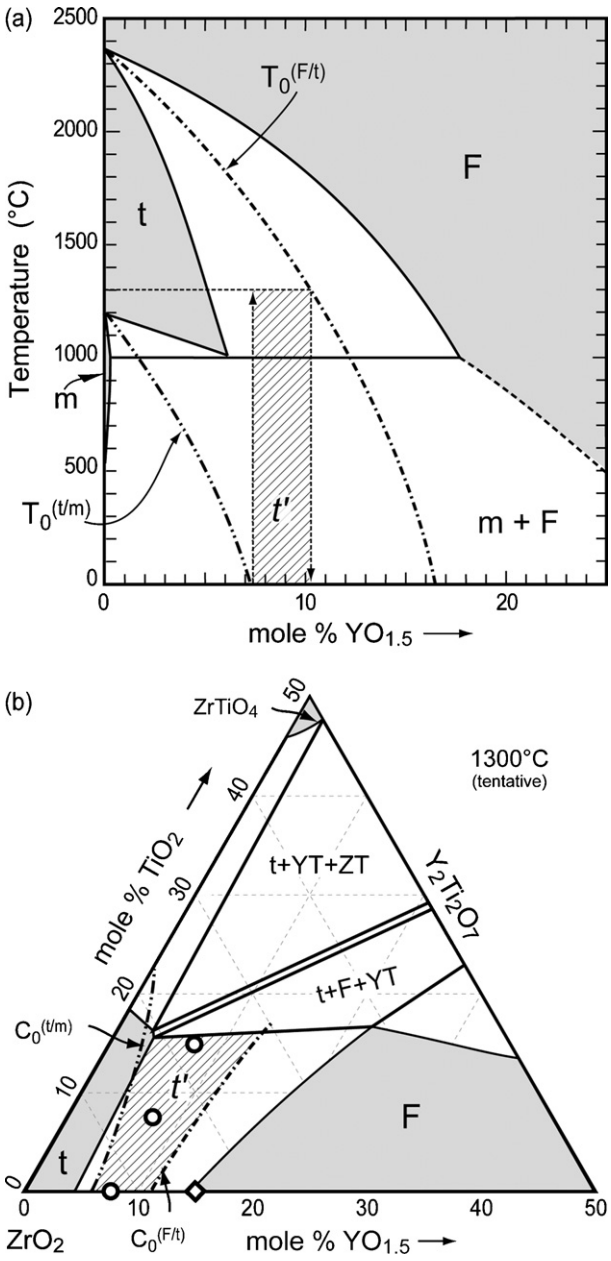

Fig. 16. (a) ZrO_2–$YO_{1.5}$ phase diagram showing the domain wherein non-transformable-tetragonal solid solutions are thermodynamically feasible and favored over the cubic form of the same composition up to 1300 °C (hatched area). (b) Extension of that domain into the ZrO_2–$YO_{1.5}$–TiO_2 system. C_0(t/m) is the trace of the T_0(t/m) surface at ambient temperature, and C_0(F/t) is the trace of the T_0(F/t) surface on the 1300 °C isotherm. Adapted from Ref. [24].

for the growth stress which, while measurable, has not been adequately rationalized or predicted.

(ii) A basic understanding of the adhesion of the α-Al_2O_3/γ-Ni interface is progressing. First principles computations based on density functional theory have demonstrated trends in the work of separation of the interface, Γ_0, upon segregation of impurities and dopants, consistent with experimental findings. A scheme for linking Γ_0 to the toughness through a crack extension simulation is in place: but results are not yet formalized because of ambiguities regarding the plasticity length scale for the bond coat adjacent to the interface.

(iii) The toughness of tetragonal oxides has been attributed to their ferroelastic properties. The dissipation that causes toughening occurs through nano-scale domain formation during crack extension, suggestive of a dependence of toughness on the tetragonality, c/a, and the coercive stress. An ensuing focus on compositions in the ZrO_2–$YO_{1.5}$–TiO_2 system having larger c/a has, indeed, led to a doubling of the toughness. While consistent with the ferroelastic mechanism, direct evidence has yet to be provided. Moreover, such enhancements suggest that systems with yet larger toughness compositions remain to be discovered.

(iv) Direct measurements of the in-plane modulus of the YSZ coatings generated by EB-PVD are still sparse. Approaches that provide further measurements while attached to the substrate and characterize trends with inter-columnar-connectivity are merited.

(v) Yielding of YSZ contributes significant to its ability to withstand impact by projectiles at high temperature. Plastic deformation also participates in kink band development during impact. A systematic assessment of the deformation mechanisms and of trends in yield strength with composition would facilitate design for impact tolerance.

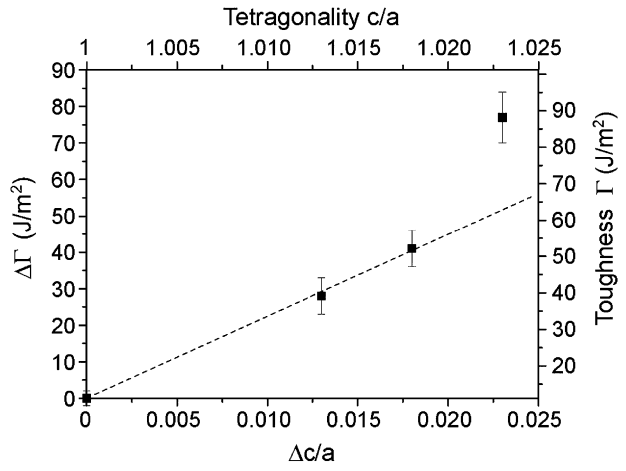

Fig. 17. Trend in toughness with tetragonality for the compositions marked in Fig. 14b.[24] From left: $15.2YO_{1.5}$, $7.6YO_{1.5}$, $7.6YO_{1.5}$–$7.6TiO_2$ and $7.6YO_{1.5}$–$15.2TiO_2$.

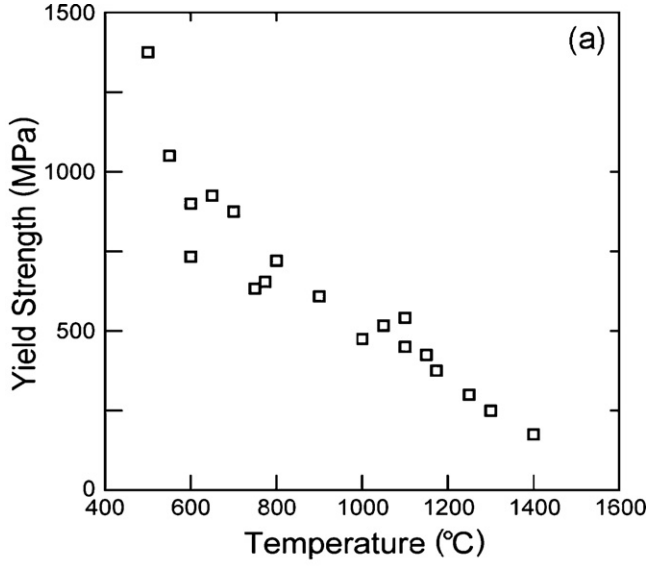

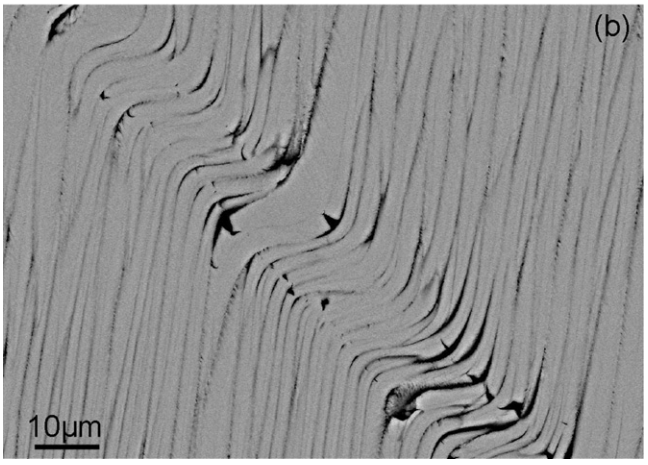

Fig. 18. (a) The yield strength of 7-YSZ as a function of temperature. (b) A kink band induced in a columnar material by impressing at 1100 °C: note the plastic bending of the 7-YSZ across the band.

Acknowledgements

This publication incorporates ideas developed under research programs sponsored by the Office of Naval Research (MURI/N00014-00-1-0438) and the National Science Foundation (DMR-0605700, DMR-0099695).

References

1. Miller, R. A., Thermal barrier coatings for aircraft engines: history and directions. *J. Therm. Spray Technol.*, 1997, **6**(1), 35–42.
2. Evans, A. G., Mumm, D. R., Hutchinson, J. W., Meier, G. H. and Pettit, F. S., Mechanisms controlling the durability of thermal barrier coatings. *Prog. Mater. Sci.*, 2001, **46**(5), 505–553.
3. Clarke, D. R., Stress generation during high-temperature oxidation of metallic alloys. *Curr. Opin. Solid State Mater. Sci.*, 2002, **6**(3), 237–244.
4. Levi, C. G., Emerging materials and processes for thermal barrier systems. *Curr. Opin. Solid State Mater. Sci.*, 2004, **8**, 77–91.
5. Clarke, D. R. and Levi, C. G., Materials design for the next generation thermal barrier coatings. *Annu. Rev. Mater. Sci.*, 2003, **33**(1), 383–417.
6. Patdture, N., Gell, M. and Jordan, E., Thermal barrier coatings for gas-turbine engine applications. *Science*, 2002, **296**, 280–284.
7. Stiger, M. J., Yanar, N. M., Toppings, M. G., Pettit, F. S. and Meier, G. H., Thermal barrier coatings for the 21st century. *Z. Metall.*, 1999, **90**, 1069.
8. Wright, P. K., Influence of cyclic strain on life of a PVD TBC. *Mater. Sci. Eng. A*, 1998, **245**(2), 191–200.
9. Mévrel, R., Laizet, J. C., Azzopardi, A., Leclercq, B., Poulain, M., Lavigne, O. and Demange, D., Thermal diffusivity and conductivity of $Zr_{1-x}Y_xO_{2-x/2}$ ($x = 0$, 0.084 and 0.179) single crystals. *J. Eur. Ceram. Soc.*, 2004, **24**, 3081–3089.
10. Maloney, M. J., Thermal barrier coating systems and materials. US Patent No. 6,117,560, 2000.
11. Maloney, M. J., Thermal barrier coating systems and materials. US Patent No. 6,177,200, 2001.
12. Vassen, R., Cao, X., Tietz, F., Basu, D. and Stöver, D., Zirconates as new materials for thermal barrier coatings. *J. Am. Ceram. Soc.*, 2000, **83**, 2023–2028.
13. Suresh, G., Seenivasan, G., Krishnaiah, M. K. and Murti, P. S., Investigation of the thermal conductivity of selected compounds of lanthanum, samarium and europium. *J. Alloys Compd.*, 1998, **269**, L9–L12.
14. Fevre, M., Finel, A., Caudron, R. and Mevrel, R., Local order and thermal conductivity in yttria-stabilized zirconia. II. Numerical and experimental investigations of thermal conductivity. *Phys. Rev. B*, 2005, **72**, 104118.
15. Stecura, S., *Optimization of the NiCrAl–Y/ZrO2–Y2O3 Thermal Barrier System, NASA TM-86905*. NASA, Cleveland, OH, 1985.
16. Fabrichnaya, O., Wang, C., Zinkevich, M., Levi, C. G. and Aldinger, F., Phase equilibria and thermodynamic properties of the ZrO_2–$GdO_{1.5}$–$YO_{1.5}$ system. *J. Phase Equilibr. Diffus.*, 2005, **26**, 591–604.
17. Winter, M. and Clarke, D. R., Oxide materials with low thermal conductivity. *J. Am. Ceram. Soc.*, 2007, **90**(2), 533–540.
18. Nicholls, J. R., Lawson, K. J., Johnstone, A. and Rickerby, D. S., Methods to reduce the thermal conductivity of EB-PVD TBCs. *Surf. Coat. Technol.*, 2002, **151–152**, 383–391.
19. Zhu, D. and Miller, R. A., Thermal conductivity and sintering behavior of advanced TBCs. *Ceram. Eng. Sci. Proc.*, 2002, **23**(4), 457–468.
20. Lehmann, H., Pitzer, D., Pracht, G., Vassen, R. and Stöver, D., Thermal conductivity and thermal expansion coefficients of the lanthanum rare-earth-element zirconate system. *J. Am. Ceram. Soc.*, 2003, **86**(8), 1338–1344.
21. Evans, A. G., Fleck, N. A., Faulhaber, S., Vermaak, N., Maloney, M. and Darolia, R., Scaling laws governing the erosion and impact resistance of thermal barrier coatings. *Wear*, 2006, **260**, 886–894.
22. Evans, A. G. and Hutchinson, J. W., The mechanics of coating delamination in thermal gradients. *Surf. Coat. Technol.*, 2007, **201**, 7905–7916.
23. Mercer, C., Williams, J. R., Clarke, D. R. and Evans, A. G., On a ferroelastic mechanism governing the toughness of metastable tetragonal-prime (t′) yttria-stabilized zirconia. *Proc. Royal Soc. Ser. A*, 2007, **463**, 1393–1408.

24. Schaedler, T. A., Leckie, R. M., Kraemer, S., Evans, A. G. and Levi, C. G., Toughening of Non-Transformable t'-YSZ by addition of Titania. *J. Am. Ceram. Soc.*, 2007, **90**(12), 3896–3901.
25. Pitek, F. M. and Levi, C. G., Opportunities for TBCs in the ZrO_2–$YO_{1.5}$–$TaO_{2.5}$ system. *Surf. Coat. Technol.*, 2007, **201**, 6044–6050.
26. Clarke, D. R., The lateral growth strain accompanying the formation of a thermally grown oxide. *Acta Mater.*, 2003, **51**, 1393.
27. Nicholls, J. R., Advances in coating design for high-performance gas turbines. *MRS Bull.*, 2003, **28**(9), 659–670.
28. Warnes, B. M. and Punola, D. C., Clean diffusion coatings by chemical vapor deposition. *Surf. Coat. Technol.*, 1997, **94-95**, 1–6.
29. Goward, G. W., Progress in coatings for gas turbine airfoils. *Surf. Coat. Technol.*, 1998, **108–109**, 1–3.
30. Boone, D. H., Strangman, T. E. and Wilson, T. E., Some effects of structure and composition on the properties of electron beam vapor deposited coatings for gas turbine superalloys. *J. Vac. Sci. Technol.*, 1974, **11**(4), 641–646.
31. Xu, T., Faulhaber, S., Mercer, C., Maloney, M. and Evans, A. G., Observations and analyses of failure mechanisms in thermal barrier systems with two phase bond coats based on NiCoCrAlY. *Acta Mater.*, 2004, **52**, 1439.
32. Rickerby, D. S. and Wing, R. G., US Patent No. 5,942,337, August 1999.
33. Gleeson, B., Sordelet, D. J. and Wang, W., US Patent 7,273,662, September 25, 2007.
34. Tolpygo, V. K. and Clarke, D. R., Surface rumpling of a (Ni,Pt)Al bond coat induced by cyclic oxidation. *Acta Mater.*, 2000, **48**, 3283–3293.
35. Tolpygo, V. K., Rumpling induced by thermal cycling of an overlay coating: the effect of coating thickness. *Acta Mater.*, 2004, **52**, 615–621.
36. Balint, D. S. and Hutchinson, J. W., An analytical model of rumpling in thermal barrier coatings. *J. Mech. Phys. Solids*, 2005, **53**, 949–973.
37. Davis, A. W. and Evans, A. G., A protocol for validating models of the cyclic undulation of thermally grown oxides. *Acta Mater.*, 2005, **53**, 1895–1905.
38. Karlsson, A. M., Hutchinson, J. W. and Evans, A. G., A fundamental model of cyclic instabilities in thermal barrier systems. *J. Mech. Phys. Solids*, 2002, **50**, 1565–1589.
39. Chen, M. W., Glynn, M. L., Ott, R. T., Hufnagel, T. C. and Hemker, K. J., Characterization and modeling of a martensitic transformation in a platinum modified diffusion aluminide bond coat for thermal barrier coatings. *Acta Mater.*, 2003, **51**, 4279–4294.
40. Johnson, C. A., Ruud, J. A., Bruce, R. and Wortman, D., Relationships between residual stress, microstructure and mechanical properties of electron beam physical vapor deposition thermal barrier coatings. *Surf. Coat. Technol.*, 1998, **108–109**, 80–85.
41. Gregori, G., Li, L., Nychka, J. A. and Clarke, D. R., Vibration damping of superalloys and thermal barrier coatings at high-temperatures. *Mater. Sci. Eng. A*, 2007, **466**, 256–264.
42. Strangman, T. E., Thermal barrier coatings for turbine airfoils. *Thin Solid Films*, 1985, **127**, 93–105.
43. Taylor, T. A., US Patent 5,073,433, 1991.
44. Bruce, R. W. and Schaeffer, J. C., European Patent EP1281788, 2003.
45. Tolpygo, V. K. and Clarke, D. R., On the rumpling mechanism in nickel-aluminide coatings. Part II. Characterization of surface undulations and bond coat swelling. *Acta Mater.*, 2004, **52**, 5129–5141.
46. Mennicke, C., Mumm, D. R. and Clarke, D. R., Transient phase evolution during oxidation of a two-phase NiCoCrAlY bond coat. *Z. Metall.*, 1999, **90**(12), 1079–1084.
47. Levi, C. G., Sommer, E., Terry, S. G., Catanoiu, A. and Rühle, M., Alumina grown during deposition of thermal barrier coatings on NiCrAlY. *J. Am. Ceram. Soc.*, 2002, **86**, 676–685.
48. Murphy, K. S., More, K. L. and Lance, M. J., As-deposited mixed zone in thermally grown oxide beneath a thermal barrier coating. *Surf. Coat. Technol.*, 2001, **146–147**, 152–161.
49. Tolpygo, V. K. and Clarke, D. R., Microstructural study of the theta–alpha transformation in alumina scales formed on nickel-aluminides. *Mater. High Temp.*, 2000, **17**(1), 59–70.
50. Pint, B. A., Martin, J. R. and Hobbs, L. W., The oxidation mechanism of theta-Al_2O_3 scales. *Solid State Ionics*, 1995, **78**, 99–107.
51. Brumm, W. M. and Grabke, H. J., The oxidation behavior of NiAl. Part 1. Phase-transformations in the alumina scale during oxidation of NiAl and NiAl–Cr Alloys. *Corros. Sci.*, 1992, **33**(11), 1677–1690.
52. Doychak, J., Smialek, J. L. and Mitchell, T. E., Transient oxidation of single-crystal beta-NiAl. *Met. Trans. A*, 1989, **20**(3), 499–518.
53. Rybicki, G. C. and Smialek, J. L., Effect of the theta–alpha-Al_2O_3 transformation on the oxidation behavior of beta-NiAl + Zr. *Oxid. Met.*, 1989, **31**(3–4), 275–304.
54. Reddy, A., Hovis, D. B., Heuer, A. H., Paulikas, A. P. and Veal, B. W., In situ study of oxidation-induced growth strains in a model NiCrAlY bond-coat alloy. *Oxid. Met.*, 2007, **67**(3–4), 153–177.
55. Heuer, A. H., Reddy, A., Hovis, D. B., Veal, B. W., Paulikas, A., Vlad, A. and Rühle, M., The effect of surface orientation on oxidation-induced growth strains in single crystal NiAl: an in situ synchrotron study. *Scripta Mater.*, 2006, **54**, 1907–1912.
56. Clarke, D. R. and Adar, F., Measurement of the crystallographically transformed zone produced by fracture in ceramics containing tetragonal zirconia. *J. Am. Ceram. Soc.*, 1982, **65**, 284–288.
57. Gong, X. Y. and Clarke, D. R., On the measurement of strain in coatings formed on a wrinkled elastic substrate. *Oxid. Met.*, 1998, **50**, 355.
58. Lipkin, D. M. and Clarke, D. R., Measurement of the stress in oxide scales formed by oxidation of alumina-forming alloys. *Oxid. Met.*, 1996, **45**(3–4), 267–280.
59. Zhang, W., Smith, J. R., Wang, X. G. and Evans, A. G., Influence of sulfur on the adhesion of the nickel/alumina interface. *Phys. Rev. B*, 2003, **67**, 245414.
60. Zhang, W., Smith, J. R. and Evans, A. G., The connection between *ab initio* calculations and interface adhesion measurements on metal/oxide systems: Ni/Al_2O_3 and Cu/Al_2O_3. *Acta Mater.*, 2002, **50**, 3803–3816.
61. Smialek, J. L., Effect of sulfur removal on Al_2O_3 scale adhesion. *Metall. Trans. A*, 1991, **22**, 739–752.
62. Ruud, J. A., Bartz, A., Borom, M. P. and Johnson, C. A., Strength degradation and failure mechanisms of electron-beam physical-vapor-deposited thermal barrier coatings. *J. Am. Ceram. Soc.*, 2001, **84**, 1545–1552.
63. Davis, A. W. and Evans, A. G., Effects of bond coat misfit strains on the rumpling of thermally grown oxides. *Metall. Mater. Trans.*, 2006, **37A**, 2085–2095.
64. Mumm, D. R., Evans, A. G. and Spitsberg, I. T., Characterization of a cyclic displacement instability for a thermally grown oxide in a thermal barrier system. *Acta Mater.*, 2001, **49**, 2329–2340.
65. Tolpygo, V. K. and Clarke, D. R., unpublished work.
66. Chen, X., Wang, R., Yao, N., Evans, A. G., Hutchinson, J. W. and Bruce, R. W., Foreign object damage in a thermal barrier system: mechanisms and simulations. *Mater. Sci. Eng. A*, 2003, **352**, 221–231.
67. Nicholls, J. R., Deakin, M. J. and Rickerby, D. S., A comparison between the erosion behavior of thermal spray and electron-beam physical vapour deposition thermal barrier coatings. *Wear*, 1999, **233–235**, 352–361.
68. Wellman, R. G. and Nicholls, J. R., Some observations on erosion mechanisms of EB-PVD TBCs. *Wear*, 2000, **242**, 89–96.
69. Bruce, R. W., Development of 1232 °C (2250 °F) erosion and impact tests for thermal barrier coatings. *Tribol. Trans.*, 1998, **41**, 399–410.
70. Borom, M. P., Johnson, C. A. and Peluso, L. A., Role of environmental deposits and operating surface temperature in spallation of air plasma sprayed thermal barrier coatings. *Surf. Coat. Technol.*, 1996, **86–87**, 116–126.
71. Mercer, C., Faulhaber, S., Evans, A. G. and Darolia, R., A delamination mechanism for thermal barrier coatings subject to calcium-magnesium-alumino-silicate (CMAS) infiltration. *Acta Mater.*, 2005, **53**, 1029–1039.
72. Krämer, S. Faulhaber, S., Chambers, M., Levi, C. G., Hutchinson, J. W. and Evans, A. G., Mechanisms of cracking and delamination within thermal barrier systems in aeroengines subject to calcium-magnesium-alumino-silicate (CMAS) penetration. *Mater. Sci. Eng. A*, in press.
73. Nychka, J. A., Quantification of aluminum outward diffusion during oxidation of FeCrAl alloys. *Oxid. Met.*, 2005, **63**, 325–352.
74. Tolpygo, V. K., Microstructural evidence for counter-diffusion of aluminum and oxygen during the growth of alumina scales. *Mater. High Temp.*, 2003, **20**, 261–271.
75. Yoshimura, M., Yashima, M., Noma, T. and Somiya, S., Formation of diffusionlessly transformed tetragonal phases by rapid quenching of melts in ZrO_2-$RO_{1.5}$ systems (R = rare earths). *J. Mater. Sci.*, 1990, **25**, 2011–2016.

76. Watanabe, M., Mercer, C., Levi, C. G. and Evans, A. G., A probe for the high temperature deformation of oxides used for thermal barrier systems. *Acta Mater.*, 2004, **52**, 1479–1487.
77. Virkar, A. V., Role of ferroelasticity in toughening of zirconia ceramics. *Key Eng. Mater.*, 1998, **153–154**, 183–210.
78. Chan, C. J., Lange, F. F., Rühle, M., Jue, J. F. and Virkar, A. V., Ferroelastic domain switching in tetragonal zirconia single-crystals microstructural aspects. *J. Am. Ceram. Soc.*, 1991, **74**, 807–813.
79. Baither, D., Bartsch, M., Baufeld, B., Tikhonovsky, A., Rühle, M. and Messerschmidt, U., Ferroelastic and plastic deformation of t′-zirconia single crystals. *J. Am. Ceram. Soc.*, 2001, **84**, 1755–1762.
80. Spitsberg, I. and Boutwell, B. A., Thermal barrier coatings with improved impact and erosion resistance. US Patent 6,869,703, 2005.
81. Miller, R. A., Smialek, J. L. and Garlick, R. G., Phase stability in plasma-sprayed, partially stabilized zirconia–yttria. In *Science and Technology of Zirconia*, ed. A. H. Heuer and L. W. Hobbs. The American Ceramic Society, Inc., Columbus, OH, 1981, pp. 241–253.
82. Schulz, U., Phase transformation in EB-PVD yttria partially stabilized zirconia thermal barrier coatings during annealing. *J. Am. Ceram. Soc.*, 2000, **83**, 904–910.
83. Rebollo, N. R., Fabrichnaya, O. and Levi, C. G., Phase stability of Y + Gd co-doped zirconia. *Z. Metall.*, 2003, **94**, 163–170.
84. Lughi, V., Transformation of electron-beam physical vapor deposited 8 wt.% yttria-stabilized zirconia thermal barrier coatings. *J. Am. Ceram. Soc.*, 2005, **88**, 2552–2558.
85. Lughi, V., Low-temperature transformation kinetics of electron-beam deposited 5 wt.% yttria-stabilized zirconia. *Acta Mater.*, 2007, **55**, 2049–2055.
86. Witz, G., Shklover, V., Steurer, W., Bachegowda, S. and Bossmann, H. P., Phase evolution in yttria-stabilized zirconia thermal barrier coatings studied by Rietveld refinement of X-ray powder diffraction patterns. *J. Am. Ceram. Soc.*, 2007, **90**, 2935–2940.
87. Cairney, J., Rebollo, N. R., Rühle, M. and Levi, C. G., Phase stability of thermal barrier oxides: a comparative study of Y and Yb additions. *Int. J. Mater. Res.*, 2007, **98**(12).
88. Krämer, S., Yang, J. Y., Johnson, C. A. and Levi, C. G., Thermochemical interactions of thermal barrier coatings with molten CaO–MgO–Al_2O_3–SiO_2 (CMAS) deposits. *J. Am. Ceram. Soc.*, 2006, **89**, 3167–3175.
89. Krämer, S., Yang, J. Y. and Levi, C. G., Infiltration-inhibiting reaction of gadolinium zirconate thermal barrier coatings with CMAS melts. *J. Am. Ceram. Soc.*, in press.
90. Leckie, R. M., Krämer, S., Rühle, M. and Levi, C. G., Thermochemical compatibility between Alumina and ZrO_2–$GdO_{3/2}$ thermal barrier coatings. *Acta Mater.*, 2005, **53**, 3281–3292.